Application of Two Phase (Liquid/Gas) Xenon Gamma-Camera to the Detection of Special Nuclear Material and PET Medical Imaging

POC and Principal Investigator - Yale: Daniel McKinsey, Associate Professor of Physics
Department of Physics
217 Prospect St.
New Haven, CT 06511
email: daniel.mckinsey@yale.edu
web: mckinseygroup.physics.yale.edu
Phone: (203) 436-4997, FAX: (203) 432-6175

Principal Investigator - UConn: Moshe Gai, Professor of Physics
Laboratory for Nuclear Science at Avery Point,
1084 Shennecossett Rd.
Groton, CT 06340-6097
email: moshe.gai@uconn.edu
web: astro.uconn.edu
Phone: (860)405 9068, Lab: 9267, FAX: 9075

ACCOMPLISHMENTS

What are the major goals of the project?

This is a new detection system concept for highly sensitive passive imaging of nuclear and radiological materials. We propose to use liquid xenon (LXe) to build and test a Compton gamma ray imaging system. LXe offers a formidable combination of easy availability, low cost, high gamma capture efficiency, and excellent energy and spatial resolution.

LXe is a bright scintillator, and charge produced in LXe by ionizing radiation can be rapidly drifted and detected. LXe has high Z and high density (3.0 g/cm^3) and therefore has high gamma stopping power (e.g., 6 cm attenuation length for 1.0 MeV U-238 gammas), thus enabling remarkably compact and efficient systems. Using LXe, uniform detectors are easily built, enabling high signal-to-noise imaging of gamma ray emitters. LXe is also readily available and reasonably inexpensive - about $1000 per kilogram, which is comparable to sodium iodide. The LXe technology has been recently shown to give 4% energy resolution (FWHM) at 662 keV gamma energy. Substantial improvement in this energy resolution is likely attainable with modest R&D effort. For good angular resolution, events in the LXe must be located to within millimeters, and this has been shown to be possible using wire readout.

While xenon must be cooled to be liquefied, the cooling requirements are modest because the required temperature (-100 C) is not very low by cryogenic standards. Highly efficient cryocoolers are commercially available for use at this temperature, and polyurethane foam may be used instead of vacuum for thermal insulation. Xenon may be stored at high density at room temperature using adsorption on activated charcoal. The detector may then be charged with liquid xenon by simply cooling the active volume while heating the charcoal.

The goal of this project is to test a LXe gamma ray imager, demonstrating and optimizing its energy resolution. The proposed development can be performed with inexpensive modifications to a LXe detector that exists at Yale University, and thus optimally leverages existing equipment, including photomultipliers, xenon, cooling system, storage system, power supplies, and readout electronics.

What was accomplished?

1. Detector assembly: The detector has been fully assembled twice; once in late summer 2012, and once in spring 2013 following voltage divider and high voltage feedthrough replacement. Internals assembly includes field cage, photomultipliers (PMTs), all five grids (anode, cathode, gate, bottom shield, and top shield), teflon reflectors, LXe fluid lines, thermometry and LXe level sensors. Figure 1 below shows various views of the assembled detector.

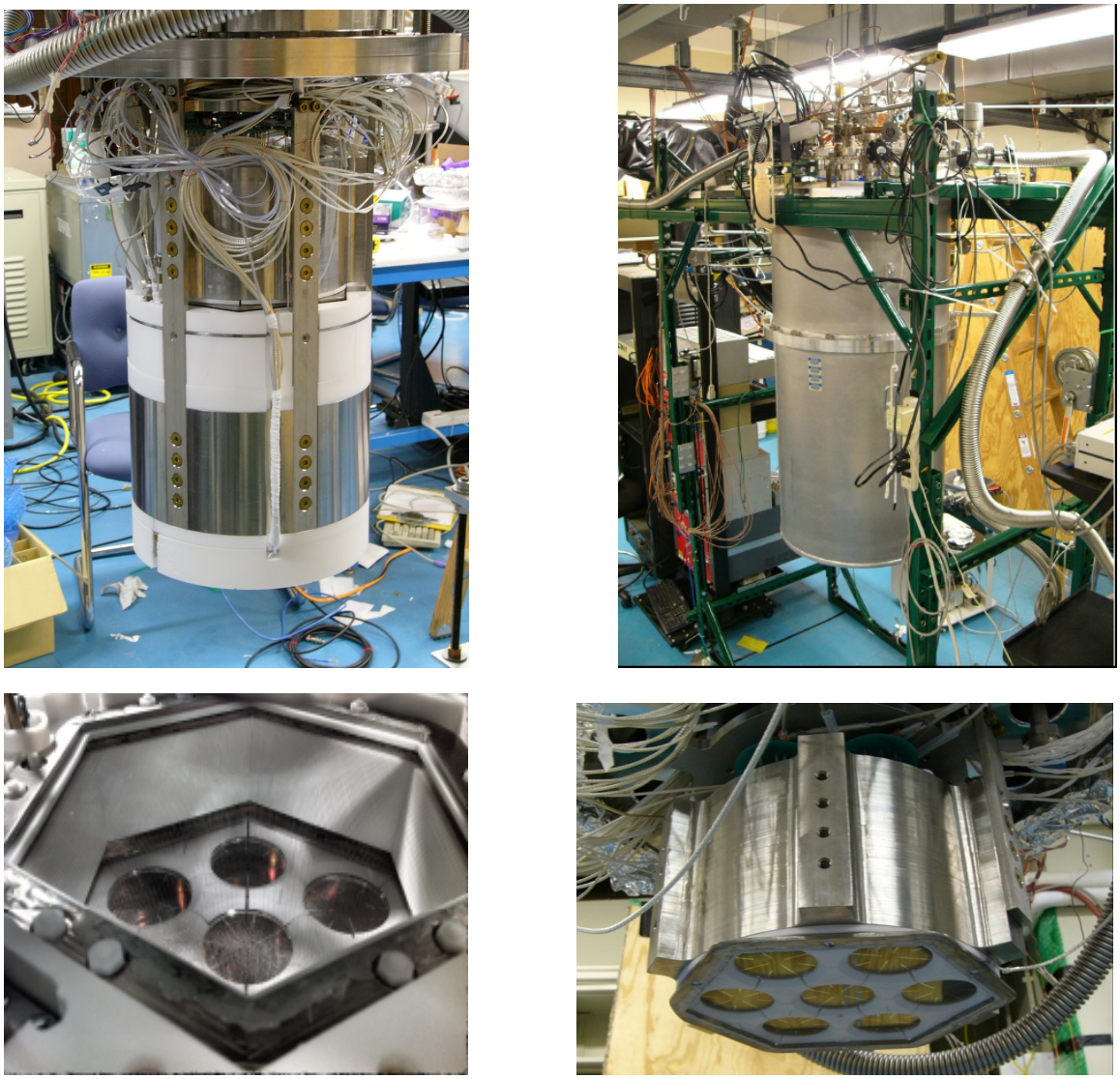

Fig. 1. **(Upper Left):** An assembled view of the detector internals, including PMTs, PTFE reflector, and field-setting grids. **(Upper Right):** The full detector, as assembled in its vacuum can. **(Lower Left):** View of the field cage and bottom PMT assembly**. (Lower Right):** View of the top PMT assembly.

2. Cryogenics: All cooling and storage systems, temperature control, and LXe level meters have been successfully operated during a commissioning run. During operation, xenon is continuously circulated at about 12 standard liters per minute (SLPM) through a getter to remove impurities diffusing into the xenon from materials in the xenon volume. To minimize cooling power, a heat exchanger has been designed to pre-cool xenon entering the detector volume using the xenon being pulled out of the volume. The heat exchanger consists of a copper pot (the evaporator) situated inside a steel vessel (the condenser) approximately 1 liter in volume. Liquid xenon leaving the main volume evaporates inside the evaporator, while gas returning from the getter enters the condenser and condenses on the vanes on the outer surface of the evaporator, subsequently raining down into the detector. Thus, heat exchange occurs across the copper wall of the evaporator. This design has been tested and shown to reduce the necessary cooling power from 10 W/SLPM to 1.5 W/SLPM for circulation rates of up to 22.5 SLPM, corresponding to 84% efficiency. A new xenon overpressure relief system was also successfully installed. Figure 2 shows a schematic of the cooling and heat exchanger system, and a photograph of this system as installed.

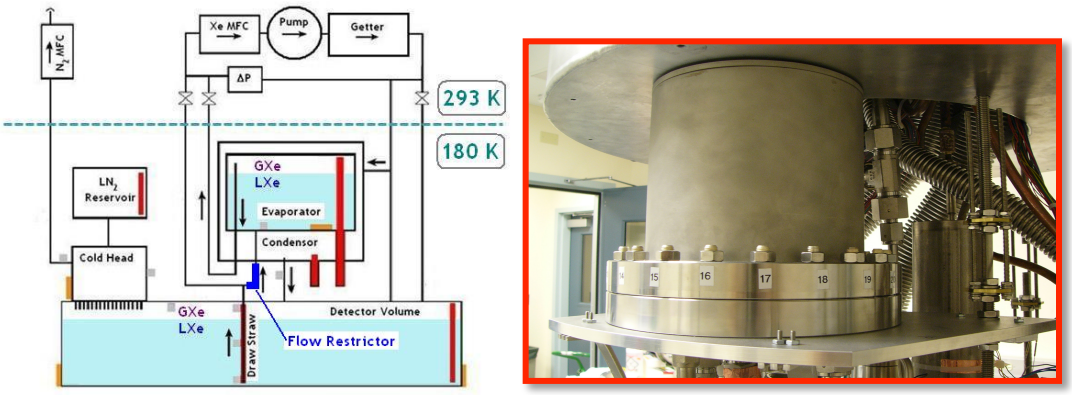

Fig. 2. **(Left):** a diagram showing the design of the cooling and heat exchanger system system. **(Right):** photograph of the heat exchanger system as installed.

3. Detector operation: Between early August and November 2012, PIXeY ran stably for three months with minimal human intervention besides filling the liquid-nitrogen reservoir every second day. All subsystems of the detector were operational. Results from this first commissioning run are noted in the sections below.

4. Xenon purification: The xenon for this project is purified using oxygen and hydrocarbon scrubbers, and by running it through a hot zirconium getter. The xenon circulation system was fixed following a bellows failure, and a system built to allow pressure monitoring of the pump interdiaphragm space to allow us to tell if a diaphragm ruptures. In our first commissioning run, a

35 microsecond electron drift lifetime was achieved, more than adequate to detect the charge signal given the 10 microsecond drift time from the cathode to gate grid. In addition, a system with residual gas analysis was built by undergraduate Evan Linck, under the supervision of postdoc Dr. Blair Edwards. This was attached to the gas handling system, using an existing residual gas analyzer left from a previous project. This system employs liquid nitrogen to remove xenon from the sample being tested, thus allowing much greater sensitivity to impurities. This will allow us to independently measure any impurities that might be compromising charge or light signal, and identify the nature of the impurities.

Fig. 3. A photograph of the purity measurement system.

5. Grids: A program of grid optimization was carried out by Nick DeStefano and Dr. Chris Wahl, resulting in a simulation of electric fields in the detector, and mechanical design of the grids to minimize grid deflection while keeping them as transparent as possible. The frame and wire material was chosen to be Monel, for its mechanical properties and easy soldering of the wires to the frame. A loom structure was built to enable winding of the grids, and a full set of grids and spares was constructed. The grids have 92% transparency, with 80 micron wire, 1 mm pitch, and 250 g/wire tension. Photographs of the grids are shown below in Fig. 4.

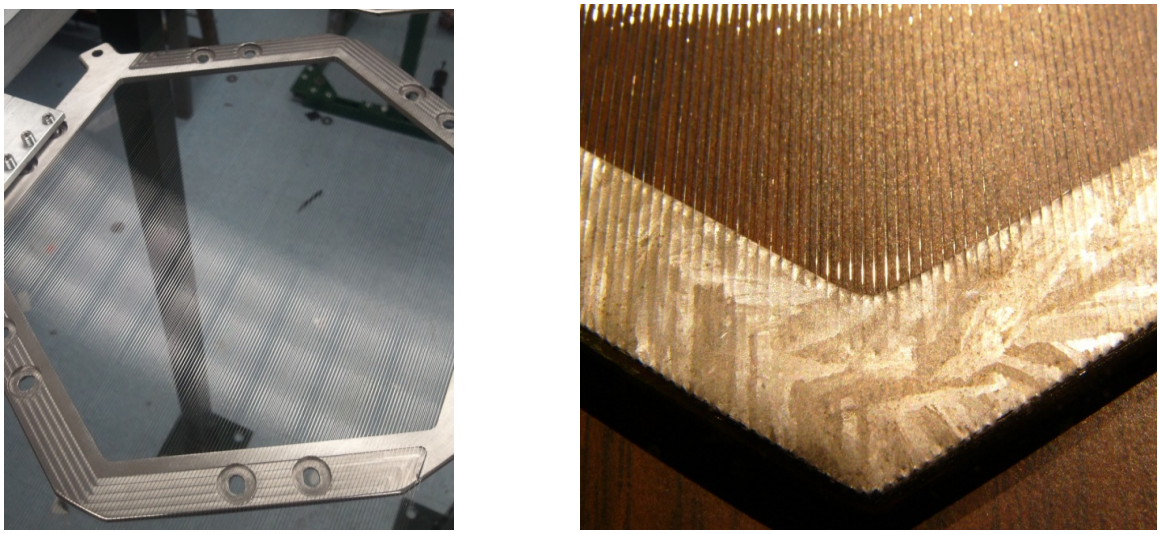

Fig. 4: **(Left)** Photograph of a Monel wire frame, with Monel wires soldered to it. **(Right)** A closeup view, showing the wire grids.

6. High voltage: In our first commissioning run, the anode and cathode voltages were limited by breakdown at their feedthroughs. These feethroughs are both located at room temperature, with one side in air and the other in xenon gas. To improve the voltages, we built special epoxy-based feedthroughs based on a design we have developed for the LUX dark matter experiment. In this design, the seal between cable and ground is made with an epoxy plug. This allows the cable to pass through the xenon gas space without any bare conductor, and should prevent breakdown for voltages up to 30 kV. A photograph of the new cathode feedthrough is shown below in Fig. 5.

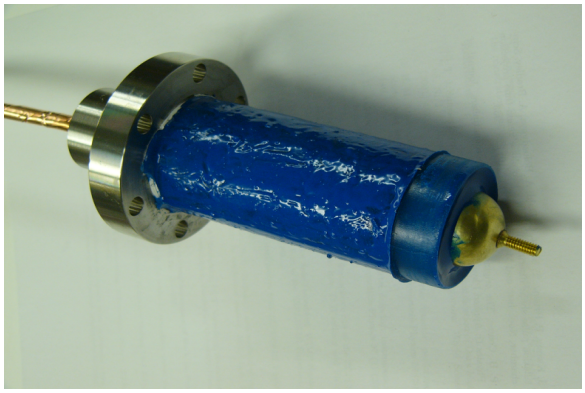

Fig. 5: Photograph of the cathode high voltage feedthrough to be used in our next commissioning run.

7. PMT testing: All PMTs have been tested by Nicole Larsen to ensure that they meet specifications for gain and quantum efficiency. These are Hamamatsu R8778 two-inch 12-stage PMTs with nominal 26% quantum efficiency, which directly detect xenon scintillation photons. The voltage divider design has been optimized for gain and linearity. Raw gain of each PMT is calibrated by finding the average area of a single photoelectron pulse. Most are operated at 1500 V and have gains of 10^6 to 10^7. In our first commissioning run, we found that the voltage dividers saturated in the proportional scintillation (S2) pulse, and this prevented measurements of energy resolution at high gamma ray energies. For our second commissioning run, we have installed new voltage dividers that have larger capacitors feeding the dynode chain, to allow higher gain. In addition, we plan to run the PMTs at lower bias voltage when taking high energy data. In Fig. 6 below are shown photographs of the PMTs and voltage dividers, as well as typical voltage and single photoelectron response.

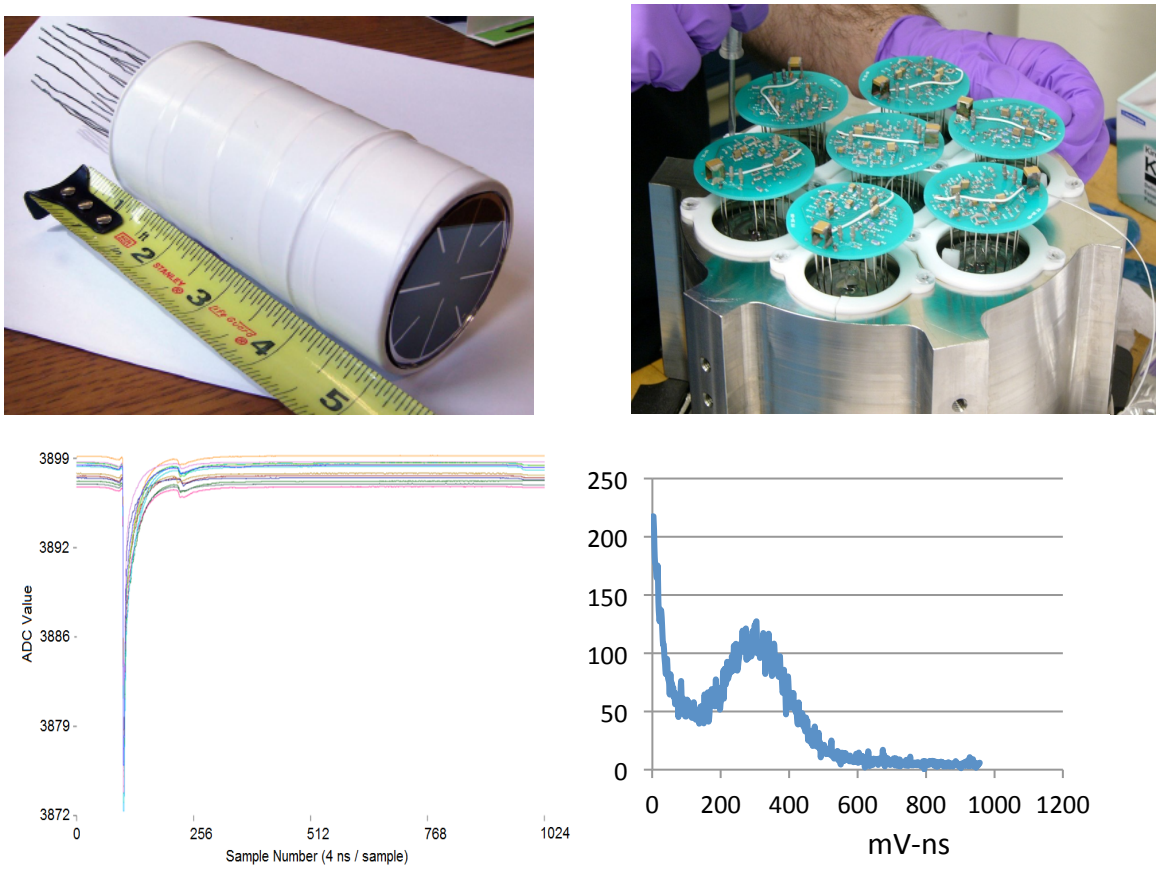

Fig. 6: **(Top Left):** Photograph of one of the Hamamatsu R8778 photomultipliers. **(Top Right):** Photograph of the voltage dividers for the top photomultiplier array. **(Bottom Left):** Typical PMT responses to prompt scintillation pulses. **(Bottom Right):** Single photoelectron response of the R8778 PMT.

8. Analysis development: To support the analysis of data from the current and future detector, Dr. Chris Wahl designed and wrote software for analysis that will be able to apply calibrations and eventually perform imaging and advanced data analysis. PIXeYCalc currently allows interfacing with the digitizers, file reading and saving, calibration, data cuts, data display, first-pass analysis, position estimation, and output into the ROOT format. It runs in parallel and is platform independent. Chris Wahl has spent much time working with graduate students Nick Destefano and Nicole Larsen as they learn to program and use PIXeYCalc.

9. Data analysis from PIXeY: Two representative measurements will be reported here. Future measurements are planned to better understand the system, especially at higher energies. Using data from gas-phase operation of PIXeY, we have observed S1 and S2 pulses in the waveforms from 13 of the 14 PMTs. Typical S1 and S2 pulses are shown in Figure 7.

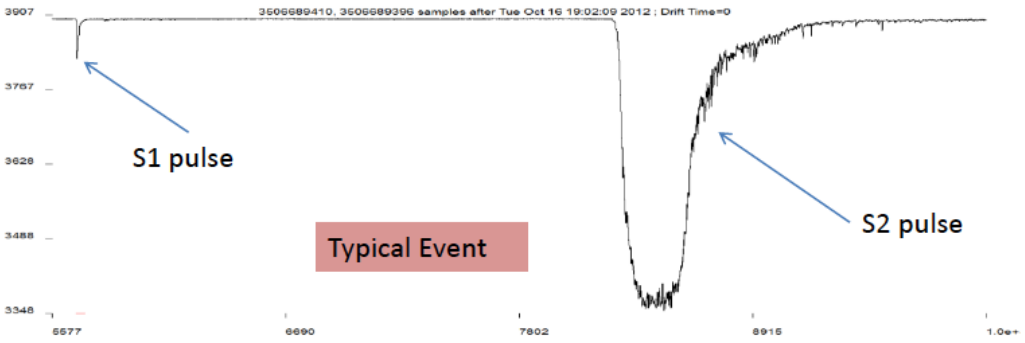

Fig. 7: Typical event in two-phase operation of our detector, showing both S1 (prompt scintillation) and S2 (proportional scintillation) pulses, separated by about 5 microseconds.

In a first measurement, a 2-μCi Co-57 source was placed on one side of the active region, outside the vacuum can, and data were recorded. For each event, the location was estimated from the center of mass of the S1 PMT signals. A histogram of counts projected onto the horizontal plane is shown in Fig. 8. It displays the familiar pincushion deformation due to the limited number of PMTs, as is often observed in Anger cameras. The events in the lower right corner of Fig. 5 are mostly due to the Co-57 source, while those on the other sides are mostly due to background events. Therefore, a region of interest was selected, as shown in the red box, to select these events. Background was subtracted, giving the spectrum in Fig. 9. From a fit of the peak at 122 keV, the energy resolution is 20%.

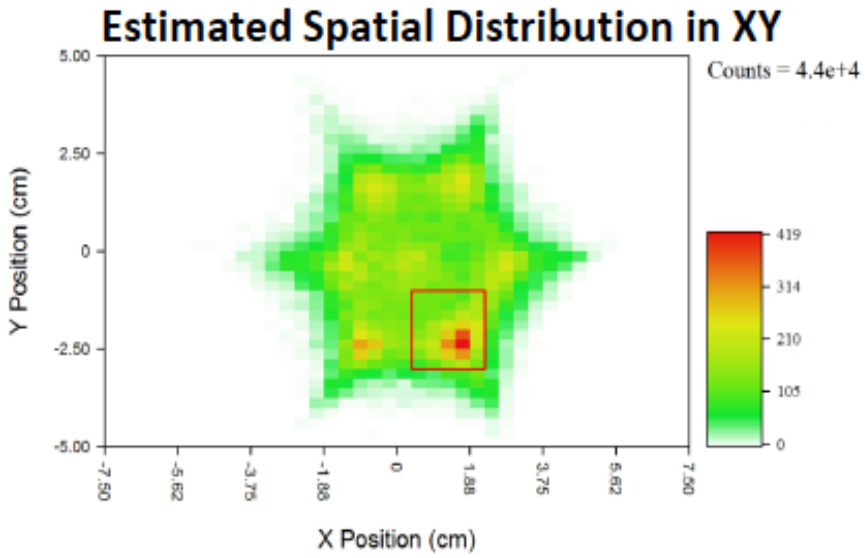

Fig. 8: Spatial distribution of Co-57 events in our detector. Events located within the red box are used for determining energy resolution (see below).

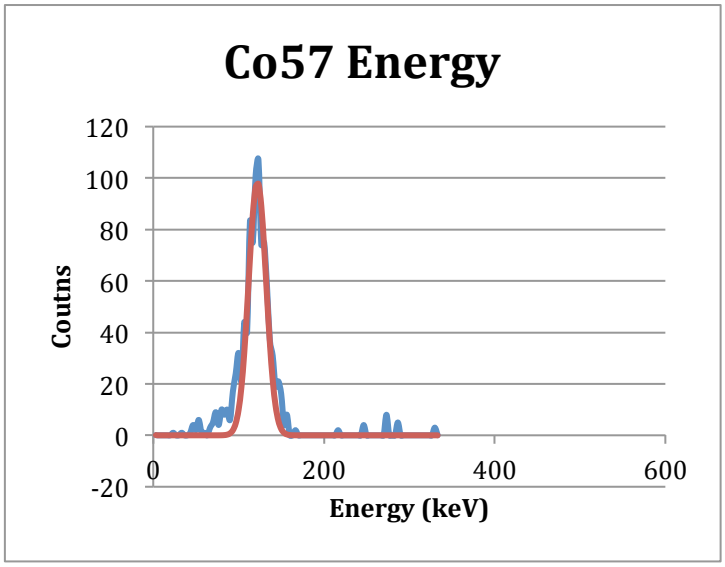

Fig. 9: Energy resolution for gamma rays emitted in Co-57 decay. A resolution of 20% FWHM was found at 122 keV.

In a second experiment, a Kr-83m source was injected directly into the LXe . Kr-83m has a 2 hour half-life, and emits two x-rays at 32.1 keV and 9.4 keV with an intermediate state lifetime of 154 ns. Therefore, the expected signal is two S1 signals with short time separation between them, and a single combined S2 signal. The source design was developed by Yale for LUX, and allows detailed mapping of the S1 and S2 response throughout the detector. Figure 10 shows the Kr-83m source hardware and PMT pulses from Kr-83m

events. In Figure 11 is shown a series of time-lapse position images, showing the Kr-83m dispersing through the detector after injection. This shows that LXe is efficiently mixing in the detector, eliminating impurities that would otherwise decrease signal strength.

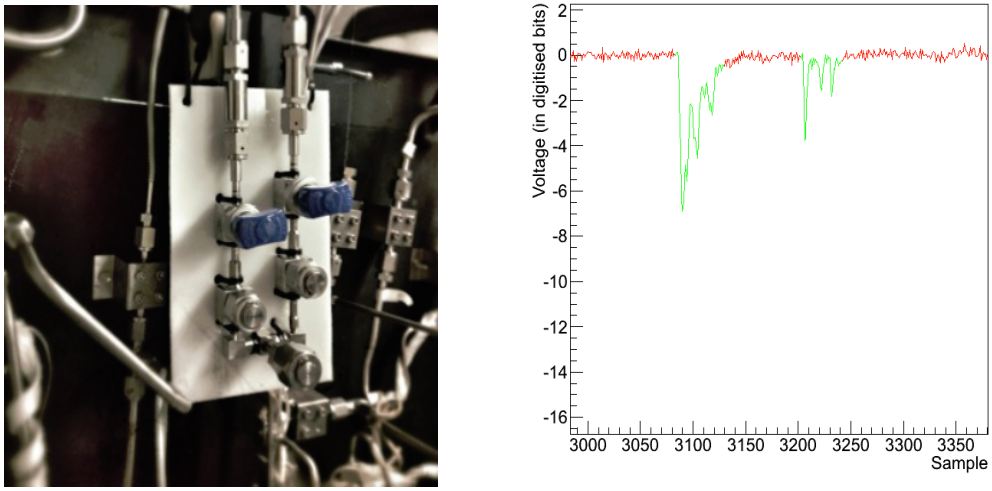

Fig. 10: **(Left)** Kr-83m source, attached to the xenon plumbing. **(Right):** Events from Kr-83m in our detector. The 32 keV and 9.4 keV pulses are evident.

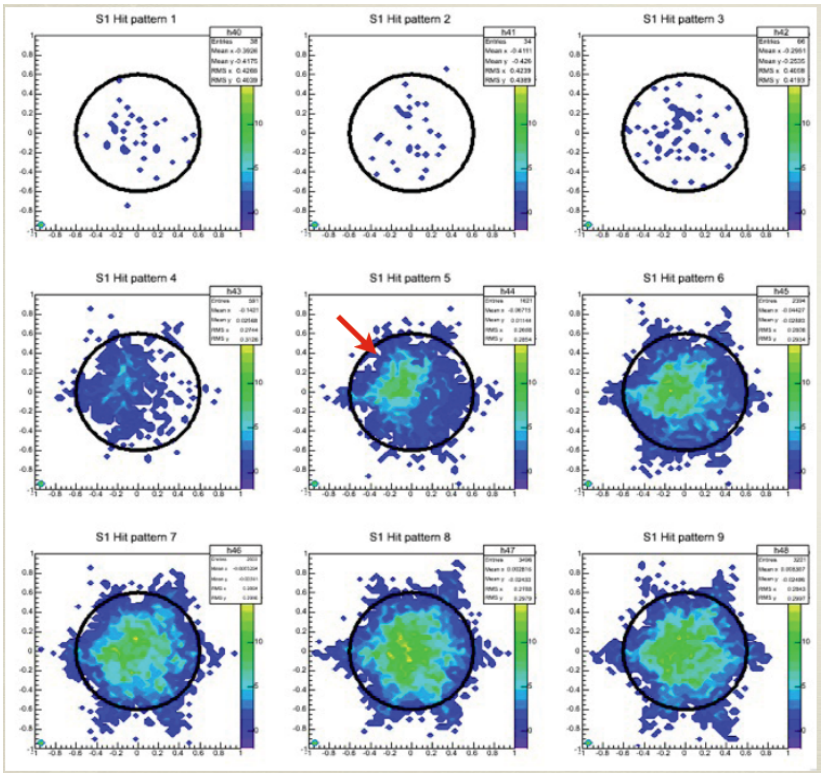

Figure 11: A series of data sets, taken over a several minutes period after addition of Kr-83m. The red arrow shows the location of Kr-83m injection.

10. Wire Readout Electronics: In the second generation PIXeY detector for Compton imaging, we plan to use crossed-wire readout to localize the electron cloud in the horizontal directions. In order to accurately gauge the lateral position of an event, PIXeY uses a set of 3 mm-pitch crossed wires on which a current is induced whenever the ionization charge from an interaction is drifted nearby. Each wire will have its own two-stage preamplifier in order to optimize noise performance while minimizing the heat load in the xenon volume. Immediately before digitization, an anti-aliasing filter is applied. This signal is then digitized to 12 bits at 2.5 MHz.

For this project we needed to design our own preamplifier because commercial preamplifiers, when placed in the xenon volume, can contaminate the xenon purity, and they are often bulky and expensive. We have followed the preamplifier design trajectory of the GeFRO system of the GERDA project. In our original design, we placed the entire preamplifier inside the xenon volume. Then, through the design process, we realized that only a small portion of the preamplifier needs to be near the sense wire; most of the preamplifier can go outside the xenon volume where there is not as much of a problem with heat load or contamination of the xenon from the circuit-board chemicals. This is a similar design step that GeFRO made to try to minimize radioactivity near their detector. We have made some significant modifications to the GeFRO design to only require one wire to leave the xenon volume per preamplifier, whereas the GeFRO design requires two wires per channel. We also have added an additional low-noise gain stage outside of the xenon volume, for a total gain of about 3000. We have performed PSPICE simulations, and tested a prototype board of a design close to the current design and found both to work as expected. Testing of the wire readout system shows noise of about 400 electrons, which is expected to drop to about 300 electrons when the system is cooled to LXe temperature.

The current design requires a JFET, capacitor, and two resistors inside the xenon volume, one transmission line to the outside, and a three-stage amplifier outside with a JFET stage, op-amp stage, and line-driver stage. This then can be connected to a CAEN digitizer (SY2791). The digitizer came with a slot for a small amplifier board at its input. Since our amplification will occur near our detector using our preamplifier, amplification here is not required. However, we still need a low-pass filter in this spot to reduce high-frequency noise and to provide protection to the digitizer's input. The full circuit is shown in Figure 12. Further tests of the wire readout electronics are planned for Summer 2013, to be performed by second year graduate student Brian Tennyson.

We have also fabricated custom wire-readout boards, for use in the new detector geometry. These frames were completed by first year graduate student Ariana Hackenburg, and soldering of wires to the boards is planned for Summer 2013.

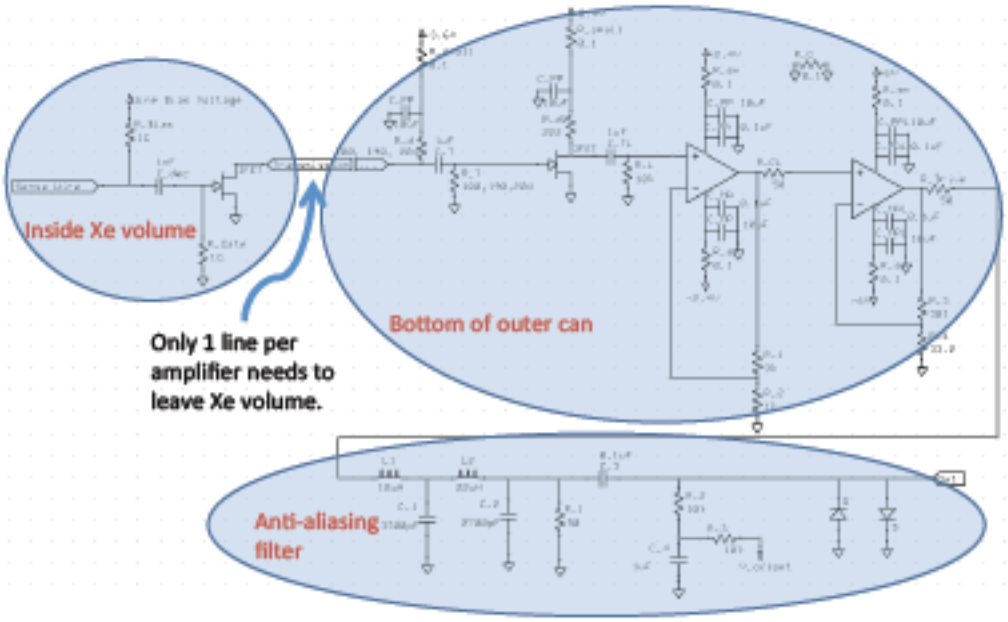

Figure 12: The complete circuit for wire readout. The part to the left of the transmission line is inside the xenon volume. The portion at the bottom is the anti-aliasing filter that goes just before the digitizer.

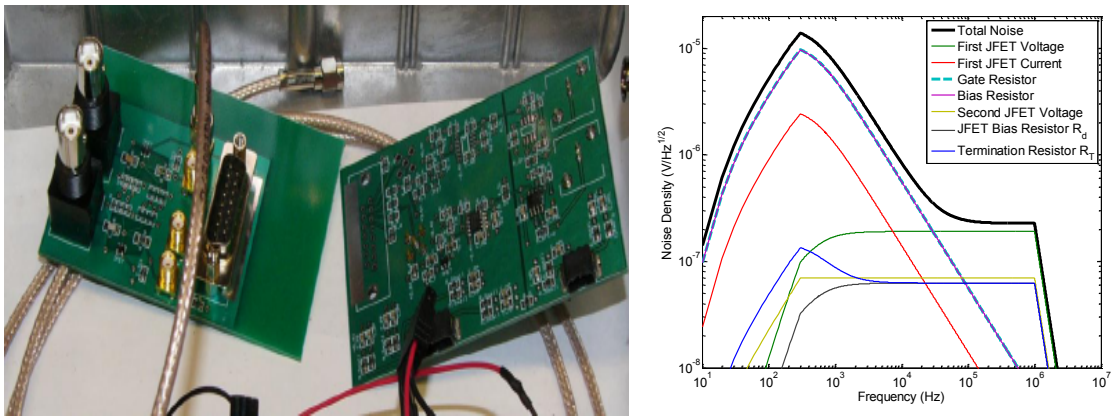

Figure 13**: (Left)** Test readout boards for the wire readout. **(Right)** Measured noise response, corresponding to about 400 electrons per channel at room temperature.

11. CAEN Electronics: The PMTs in the current and future PIXeY system will be read out with CAEN digitizers (V1720, 250 MHz, 12 bit). We identified hardware problems with one digitizer card and the interface card. One problem was in aligning the samples of the first and second digitizer cards. We set up a clock connection between the cards and a trigger connection to start the cards simultaneously. However, due to firmware problems, there is a variable delay between the cards on different runs of up to 50 ns. After iterating with CAEN, they were able to fix this problem in the case where a

simultaneous trigger starts both cards. We are currently running with a pulser input into the last channel of each card and a software routine to find the variable delay. We have been able to associate events between cards even when some events from one of the cards may be missed due to dead time, by using a software routine. We have written a program that can interface with the CAEN digitizers through a Struck-brand PCI card, which required writing a library to communicate between the card and digitizer. The program allows us to set a multitude of options and readout and view or save the results through a graphical user interface. We also set up a large shared drive to save the data and allow everyone on the PIXeY project to access it from their own computers for analysis.

12. Mechanical design: We have completed the mechanical design of the new Compton imager, and ordered the new vacuum can and liquid xenon vessel. As noted above, the new grid frames are built, with wire grids to be soldered Summer 2013 by Ariana Hackenburg. Fabrication of optical modules is planned for Summer 2013. This mechanical design work was done by Brian Tennyson, supervised by Dr. Ethan Bernard. CAD drawings and renderings of the new detector design are shown in Figure 14.

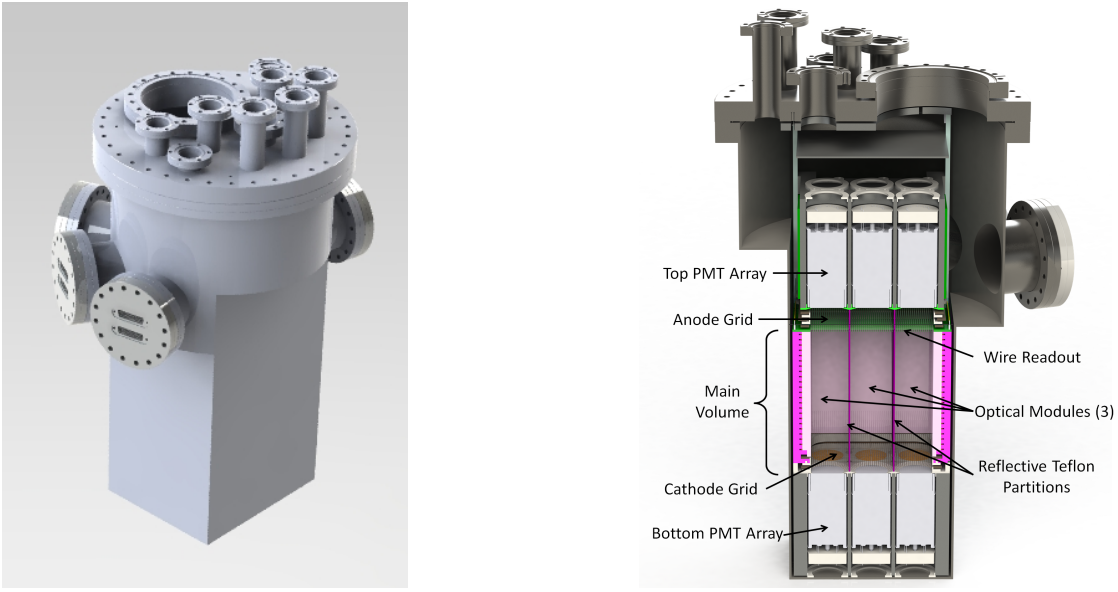

Figure 14: SolidWorks renderings of the new Compton imager internals, which are currently under fabrication. The detector will contain 18 photomultipliers (9 on top and 9 on bottom), divided into three optical volumes. One side of the can has a minimum of material so as to attain the best efficiency for gamma ray collection. Other sides of the can have had feedthroughs added for wire readout.

13. Compton imaging simulation: A simulation was performed by Chris Wahl, using Geant4 to include gamma-ray physics, surrounding materials, 1-mm position resolution, and the expected energy resolutions for interactions within separate or the same optical module. The resulting event list for a 1-MeV parallel-beam source was used to reconstruct a simple back-projection Compton image, as shown in Fig. 11. The point source was reconstructed in the correct direction and has a FWHM of only 10.8°. Sources off to the side have poorer angular spread by several degrees due to the asymmetric nature of the 3-rectangle segmentation.

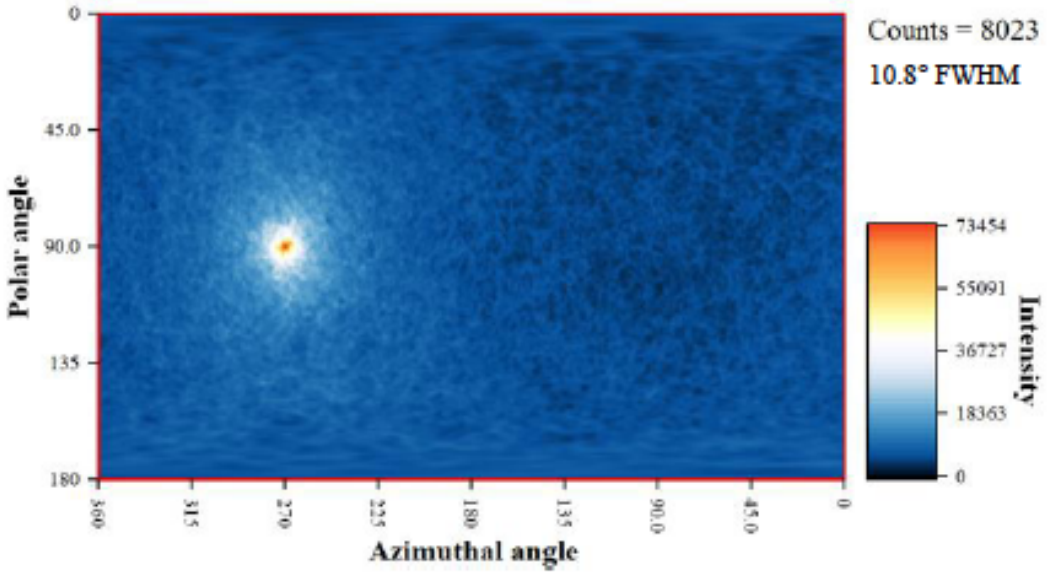

Fig. 15. The simulated Compton image for a 1-MeV point source in front of the new PIXeY detector. The angular FWHM is 10.8°.

14. Monte Carlo: Over the past year, the first generation detector was simulated with Monte Carlo. This will allow data to be compared with simulation when studying data on neutron/gamma discrimination and energy resolution. This work was being carried out by undergraduate Casey Rhyne, under the supervision of Dr. Blair Edwards. In Figure 16 can be seen the GEANT4 geometry built for these simulations, and an example optical photon simulation, showing the expected internal reflection of LXe simulation light from the liquid-gas interface.

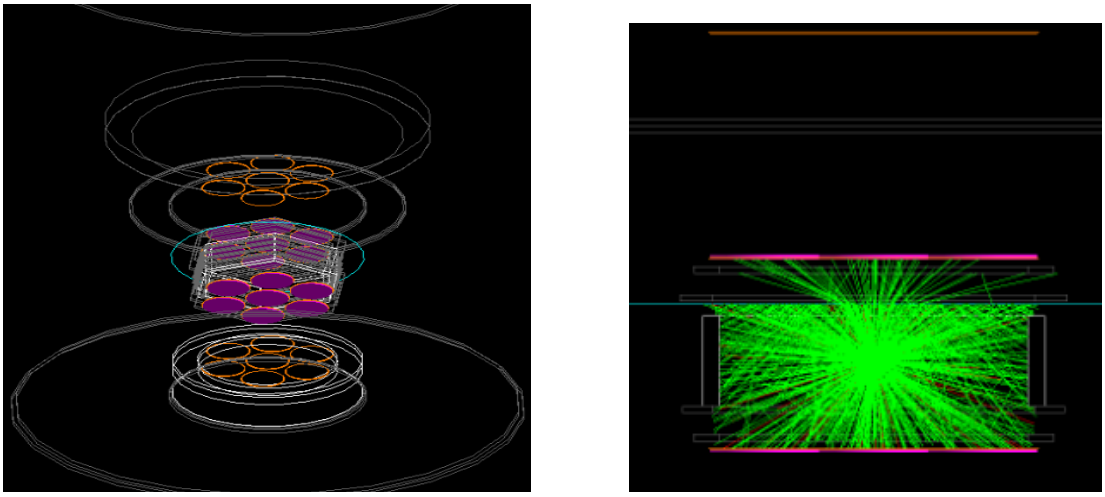

Fig. 16: **(Left):** Visible components of the entire finalized PIXeY geometry. Four of the five grid frames (gray) are visible in their proper locations, the Teflon paneling (white) surrounds the liquid xenon radially while the PMT windows (pink) are positioned above and below the active volume. **(Right):** A side-view of the detector geometry during an event simulation. Various photons (green) traverse through the detector volume. The blue line, representing the xenon gas-liquid phase boundary, demonstrates the high internal reflection within the liquid.

One of the main goals of this simulation package is to predict the photomultiplier hit pattern for various event positions. This in turn can be used to produce enhanced position reconstruction simply through optical photon detection. In Figure 17 below can be seen the simulated photon collection for two different PMTs, for a range of event positions in x, y, and z. Figure 18 shows the simulated light collection efficiencies for both top and bottom PMT arrays, as a function of event position.

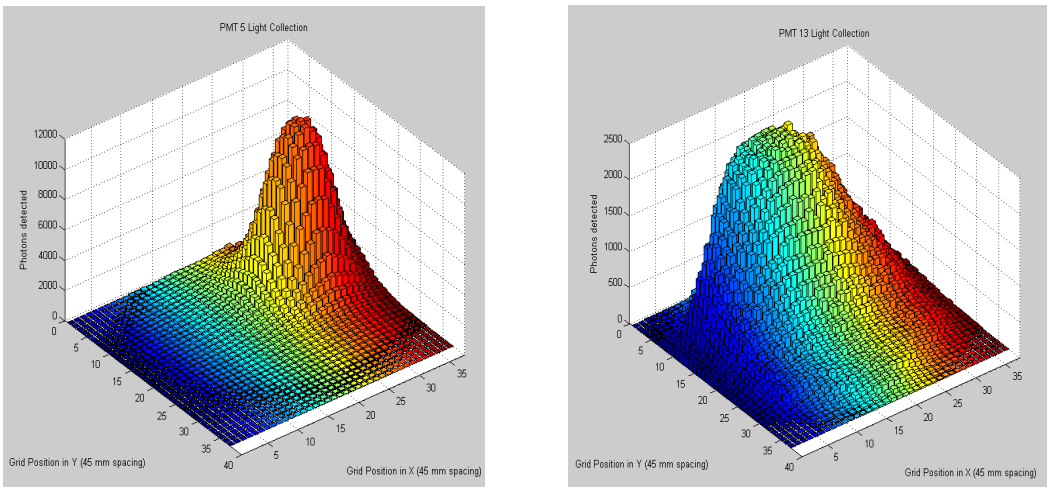

Fig. 17: S2 Light collection profile for an upper array side PMT (PMT 6). The upper array has a focused light collection profile, likely due to the short travel-distance and the lack of a reflective liquid-gas boundary below the array. Fig. 8C: S2 light collection profile for a lower array side PMT (PMT 13). The profile for the lower array is more spread out, likely as a result of the larger volume, the more distant source and the total internal reflection of the liquid-gas xenon boundary.

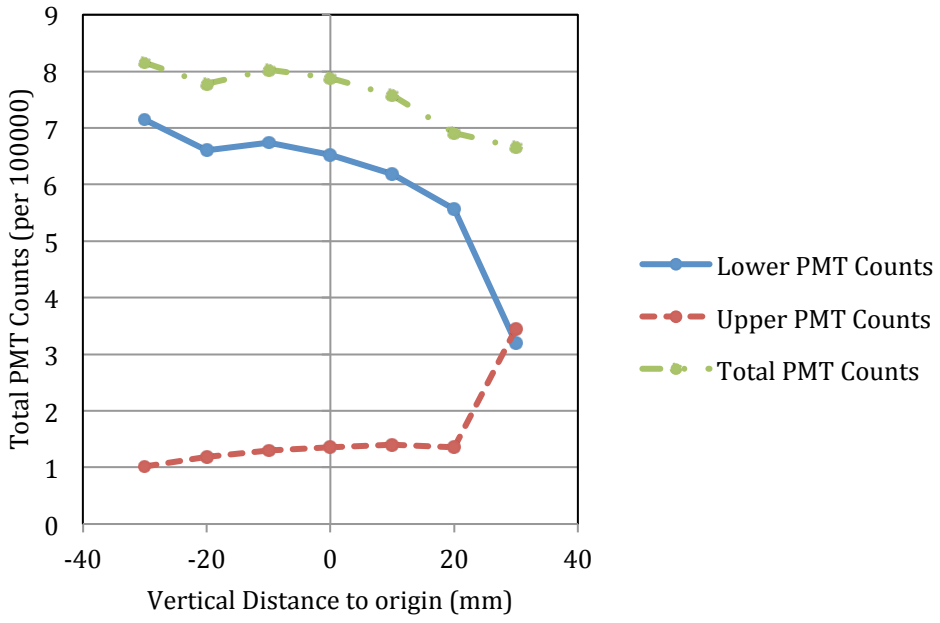

Fig. 18: The total number of photons counted in the upper and lower arrays as a function of height in the liquid xenon. The phase boundary rests between 20 mm and 30 mm, and the jump in light collection in the upper array represents the transition into the S2 light collection values in the gaseous xenon.

Finally, we simulated the predicted S2 to S1 ratio for both gamma rays and neutrons, using the NEST simulation package and our GEANT4 geometry. As expected (see Figure 19), the number of electron recoil points located below the center of the neutron recoil band decreased with increasing field. We expect to test this prediction experimentally in the upcoming data run (Summer 2013), thus learning how to optimize neutron detection with liquid xenon.

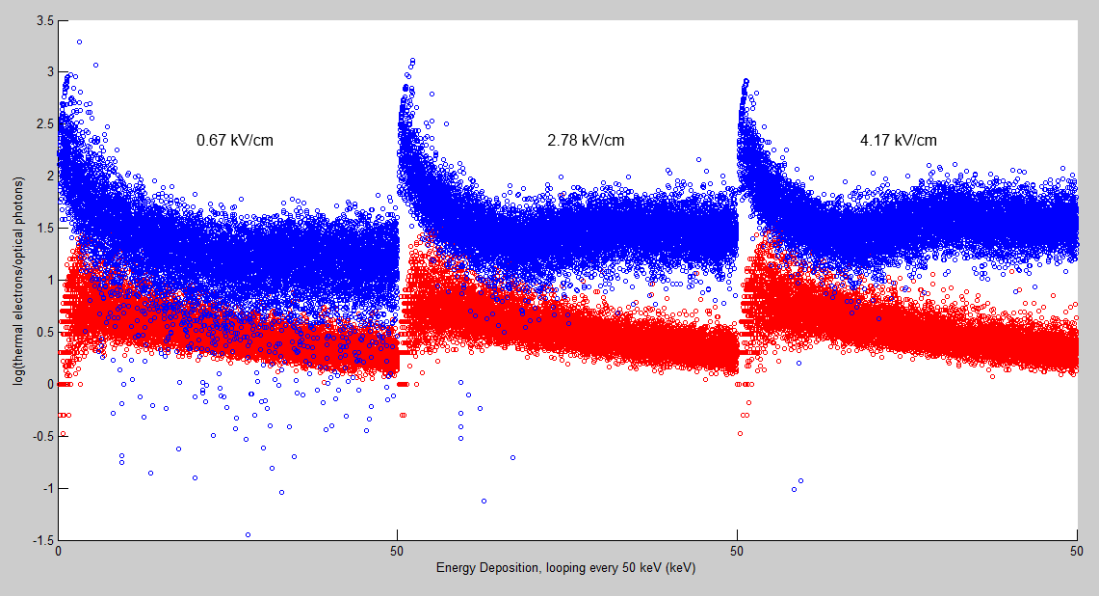

Fig. 19: Electron Recoil (blue) and Neutron Recoil (red) bands for increasing drift fields. As the electric field increased, the electric recoil band lower bound rose and became more tightly defined.